Journal of Mechanical, Civil and Industrial Engineering
ISSN: 2710-1436
DOI: 10.32996/jmcie
Journal Homepage: www.al-kindipublisher.com/index.php/jmcie

JMCIE
AL-KINDI CENTER FOR RESEARCH AND DEVELOPMENT

| RESEARCH ARTICLE

Finite Element Formulation and Computation of Superplastic Metal Forming Processes with Optimized Rate of Deformation Control

Agus Hadi Santosa Wargadipura[1] ✉ Dedi Priadi[2] and Isdaryanto Iskandar[3]

[1]*Research Centre for Advanced Material, National Research and Innovation Agency (BRIN), KST BJ Habibie, Puspiptek, Serpong, Banten 15314, Indonesia*

[2]*Department of Metalurgy and Material, Faculty of Engineering, Depok Campus, University of Indonesia*

[3]*Department of Mechanical Engineering, Atma Jaya Catholic University, Jakarta, Indonesia*

Corresponding Author: Agus Hadi Santosa Wargadipura, **E-mail**: agus005@brin.go.id

| ABSTRACT

Superplastic forming (SPF) is a material forming technique that uses superplastic exceptional elongations and deformation characteristics to form superplastic materials into certain shapes. The combination of superplastic forming with diffusion bonding (SPF/DB) gives rise to an almost unlimited extension of superplastic forming since more integral lightweight cellular structural components can be manufactured. This paper discusses numerical modelling of the mechanism of superplasticity in metallic materials. The SPF computational method based on the finite element technique augmented with the controlling rate of deformations is developed to examine a range of design or operating conditions leading to more economical forming processes. The non-Newtonian 'viscous flow' material is used to model the constitutive of superplastic material during the forming period. The contact mechanics between the sheet material and the mold surface and the intersheet material contact mechanics are imposed using the penalty control method, in which the sticking contact boundary conditions are employed. The space discretization is carried out using the membrane element under plane strain and axisymmetric flow stress conditions, while the implicit time integration technique is utilized to follow the shape changes of the formed sheet material. The validation of the SPF finite element formulation was performed by comparing it with the available analytical solution of Hydraulic Free Bulging of Thin strips. The SPF of a hemispherical dome made of 7475 aluminum sheet alloy was performed to demonstrate the forming process as well as to validate the results obtained between the SPF finite element numerical simulation and the experimental results. The SPF/DB of the multicell component section is considered in the final part.

| KEYWORDS

Superplasticity, superplastic metal forming (SPF), diffusion bonding (DB), non-Newtonian viscous flow formulation, optimized rate of deformation control, finite element method

| ARTICLE INFORMATION

ACCEPTED: 08 November 2023 **PUBLISHED:** 11 December 2023 **DOI:** 10.32996/jmcie.2023.4.4.8

1. Introduction

1.1 Phenomena of Superplasticity

Superplasticity is a term related to the behaviour of some alloys that, when deformed in tension at a particular temperature and strain-rate, exhibit very high elongations [Padmanabhan et al. 1980, Pearce 1987, Valiev et al. 2010, Kawasakia et al. 2015]. Elongations for superplastic materials are typically 200 percent to 1000 percent, but elongations as much as 5000 percent can also occur and have been reported in reference 2. This exceptional elongation is because, unlike conventional ductile metals, superplastic materials are much less susceptible to strain localization [Padmanabhan et al. 1980, Pearce 1987, Valiev et al. 2010, Ghosh et al. 1982]. Superplasticity can broadly be divided into two categories: 'Structural' or 'Isothermal' superplasticity and

'Environmental' or Cycling superplasticity[1]. The first consists of the inducement of superplasticity in materials possessing both a stable and ultrafine grain size at the temperature of deformation T ≥ 0.5T, where T is the absolute melting point of the superplastic metal alloy. The second consists of the inducement of superplasticity in material subjected to special environmental conditions, e.g. the alloy must be capable of being thermally- cycled through a phase change. Although the 'environmental' superplasticity is metallurgically interesting, it seems that this category has less potential for industrial applications compared with 'structural' superplasticity. In this paper, only the first category will be addressed. It appears that Rosenhain, Haughton and Bingham, in 1920, were the first to have chanced upon a form of structural superplasticity while experimenting with a near-ternary eutectic of zinc, aluminium and copper[1]. The elongations on the order of 60% were recorded. Later, Jeffries and Archer [1] commented on their work and attributed the effect to the presence of a very fine grain size, which is now considered a necessary condition for structural superplasticity. One of the next developments that took place in 1934 was due to the study by Pearson of tin-lead and bismuth-tin eutectic alloys[1] under both constant load and constant stress conditions. Practically, neck-free elongations of up to 650% were experienced in his first set of experiments and in his second set of tests, the maximum elongation of 1950% was recorded using a mechanism for load reduction at regular intervals. This famous result, as seen in Figure 1, has since been included in many reviews of superplasticity[Padmanabhan et al. 1980, Pearce 1987].

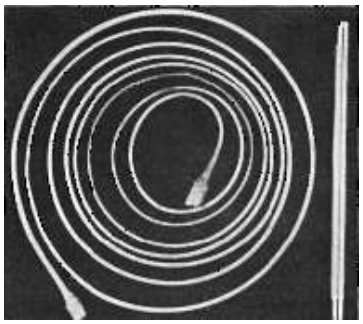

Figure 1. A tensile elongation of 1950% without failure for a Bi-Sn alloy[Padmanabhan et al. 1980]

During this period, Cook shows an empirical equation of the data of Pearson[Padmanabhan et al. 1980], as follows:

$$S = S_o + C\,V^{1/2} \quad (1)$$

Where S is the flow stress, S_o and C are constants, and V is the flow velocity, which is now known as the strain rate. There was a gap of more than ten years from this period. The revival of interest in structural superplasticity was due to Bochvar and Sviderskaya[1] when they reported the structural superplasticity of Zn-Al alloys in 1945. Another gap occurred until 1960 when Presnyakov and his co-workers [Padmanabhan et al. 1980] reported a number of new superplastic systems. However, both developments were shown to be inadequate [Padmanabhan et al. 1980]. Finally, the culmination was a review paper by Underwood [Padmanabhan et al. 1980] in 1962 that aroused considerable interest in superplasticity and stimulated research activities in this area. This led to the paper of Backofen, Turner and Avery[1] in 1964, which was concerned with superplasticity in a zinc-aluminium near eutectoid alloy. The paper also described a well-known relationship for superplastic flow in the form of [Padmanabhan et al. 1980]

$$\sigma = K\dot{\varepsilon}^{m} \quad (2)$$

Where σ is the flow stress, $\dot{\varepsilon}$ is the effective strain rate, m is the strain rate sensitivity index, and K is a material constant. It should be noted here that K and m are both constants dependent on test parameters such as temperature and grain size. The strain-rate sensitivity index, m, has considerable significance in determining the stability of flow. In the next section, we will discuss the superplastic deformation and its main parameters needed for modelling the thin sheet superplastic forming.

1.2 Superplastic Forming and Diffusion Bonding

Superplastic forming (SPF) has been described as 'the first truly new method of making things since the industrial revolution', and it is mainly dominated by the forming of thin sheets[Hamilton 1987, Al-Naib 1970, Pearce 1986, Hamilton 1977, Ghosh 1982, Hamilton 1988]. Superplastic forming is carried out at a temperature of approximately half the absolute melting temperature[Padmanabhan et al. 1980, Hamilton 1977, Hamilton 1988, Leodolter 1986] (925°C for Ti-6Al-4V), at a strain rate between 10^{-5} and 10^{-3} $sec^{-1,}$ during which relatively low stresses develop [Valiev et al. 2010, Kawasakia et al. 2015, Hamilton 1987, Ghosh et al. 1979, Kaibyshev et al. 2006]. Basically, the forming operation consists of clamping the edges of the sheet and a pressure differential is applied across a superplastic diaphragm, thus causing the material to form into a die configuration without

fracturing, as illustrated in Figure 2(a). Gas pressure, particularly argon gas, is by far the most popular in SPF [Kawasakia et al. 2015, Hamilton 1987, Al-Naib et al. 1970, Pearce 1986, Hamilton 1977, Stephen 1986, Stephen 1987].

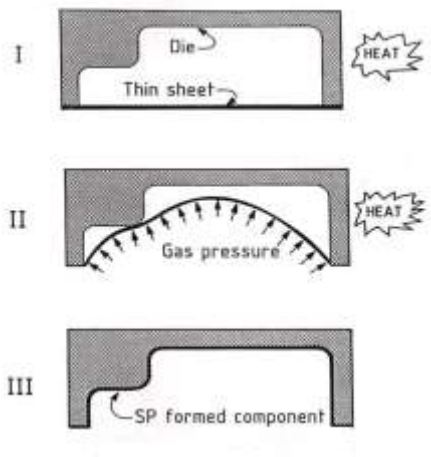

Figure 2(a). Typical Superplastic Forming Process

For a material to be potentially superplastic, it must have a very fine grain size, typically on the order of 10 microns [8,9,10,19]. Furthermore, it is evident that the constitutive law for superplastic deformation is influenced by the grain size, which grows during the forming process [Ghosh 1982, Ghosh 1979, Kaibyshev et al. 2006]. Grain size is determined by both static and deformation-enhanced grain growth, the former being a function of time at a given temperature, while the latter depends primarily on the strain rate [Padmanabhan et al. 1980; Pearce, 1987; Ghosh et al. 1982]. There are several commercial alloys suitable for superplastic forming. Particularly, Titanium alloys Ti-6Al-4V, Aluminum 7475, and Supral alloys [Pearce, 1987, Kawasakia et al. 2015, Hamilton 1987, Stephen, 1987, Jin 2019] are quite superplastic and commercially available, with the titanium alloy Ti-6Al-4V being the main material used in aerospace industries[Valiev et al. 2010, Askeland 1984, Leodolter 1986, Stephen 1986, Stephen 1987]. In the case of aluminum alloys[Pearce, 1987, Jin 2019], the main superplastic parameters for aluminum alloys are shown in Table 1.

Table 1. Superplastic Aluminum Alloys[2]

Aluminium Alloys	**Superplastic Temperature** (º Celcius)	**Optimal Superplastic Strain Rate** (Second^{-1})	**Strain rate sensitivity index, m**	**Elongation** (%)
Supral 220 (2204) Al-6Cu-0,4Zr-0.3Mg-0.2Si-0.1Ge	400 – 480	5.10^{-4} – 10^{-2}	0.45-0.7	Up to 1800
Aluminium 2090 Al-2.7Cu-2.2Li-0.7Mg-0.12Zr	510 – 530	10^{-4} – 10^{-2}	0.4 – 0.6	400 – 800
Formal 545 Al-5.5Zn-2.5Mg-1.5Cu-0.2Cr	480 – 550	5.10^{-4} – 2.10^{-2}	0.4 – 0.65	400 – 670
Aluminium 7475 Al-5.5Zn-2.5Mg-1.5Cu-0.2Cr	515 – 525	2.10^{-4} – 10^{-3}	0.5 – 0.8	Up to 1400
Aluminium 8090-SPF Al-2.5Li-1.2Cu-0.6Mg-0.1Zr	500 – 540	2.10^{-4} – 2.10^{-3}	0.4 – 0.6	500 – 1000

The main attractiveness of this forming method is that it is capable of radically extending the limitations associated with the more conventional processes, which normally require multipiece assemblies to manufacture a single component. Using SPF technology, it is now possible to form deep and complex-shaped components in one-piece and single-operation pressings without fracturing, thereby producing light, strong and more integral structural components. Consequently, the cost savings of this method are mainly based on high material utilization, reduced part/fastener count and low assembly costs. Due to the slow cooling of the component, it appears that residual forces are not significant, and consequently, the elastic spring back effect is not a problem. This is obviously another desirable quality of SPF processes. Moreover, recent developments have demonstrated that the combination of SPF with available joining methods, such as diffusion bonding (DB) [Leodolter 1986, Stephen 1986, Williamson 1986, Friedrich et al. 1988, Maehara et al. 1988], see Figure 2(b), gives rise to an almost unlimited extension of SPF [Kaibyshev et al. 2006, Kyung et al. 2015].

The combined superplastic forming (SPF) with diffusion bonding (DB) joining method is usually abbreviated SPF/DB. Recently, SPF/DB processes have gained significant importance in aerospace industries since more integral lightweight cellular structural components can be manufactured, and in the case of titanium alloy, parent metal strengths are maintained [Askeland 1984, Stephen 1987, Friedrich et al. 1988]. Using SPF/DB processes, it is now possible to produce a number of complex SPF/DB structures [Leodolter 1986, Stephen 1986, Stephen 1987, Williamson 1986, Friedrich et al. 1988].

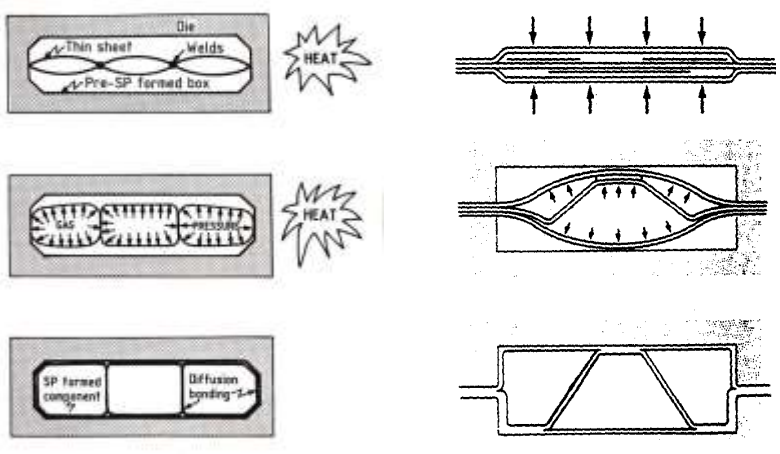

Typically, four-sheet SPF/DB Process Typically, three-sheet SPF/DB Process

Figure 2(b) Typical Superplastic Forming/Diffusion Bonding Process [Leodolter 1986, Stephen 1986, Bonet et al. 1989].

SPF/DB parts are produced by joining several sheets in a specific pattern and then superplastically expanding the sheets to produce an integrally- stiffened structure. The most common SPF/DB approaches are 2-sheet (hat stiffened structures), 3-sheet (truss-core structures) and 4-sheet (rib-stiffened structures). However, an unlimited number of configurations are possible. ManySPF and SPF/DB-formed structural components have now been successfully integrated into either civil or military aircraft [Stephen 1986, Stephen 1987, Williamson 1986, Friedrich et al. 1988]. For example, this modern forming technique has been utilized to manufacture the wing access panels (SPF) in the Airbus A310-300 series, the escape hatch door (four-sheet SPF/DB) in the BAe 125/800 series aircraft, the nozzle fairing (two-sheet SPF/DB) in the military F-15 aircraft and engine components [Stephen 1986, Williamson 1986, Friedrich et al. 1988]. Various aircraft structural components [Leodolter 1986, Stephen 1986, Williamson 1986, Friedrich et al. 1988, British Aerospace, 1992] that are successfully manufactured using superplastic forming (SPF) and concurrent superplastic forming/diffusion bonding (SPF/DB) are depicted [British Aerospace, 1992] in Figure 3.

Leading Edge Slat (SPF/DB Titanium)

Module Door

Four Sheet Sine Wave 'X' SPF/DB made component.

Figure 3. Superplastically formed and diffusion bonded aero-structure components [Stephen 1986, British Aerospace, 1992]

The cost savings of SPF and SPF/DB processes, in comparison with other conventional fabrication methods, could reach values of 30 to 60 percent, which has been substantiated by a wide range of design-to-cost studies by major aerospace companies [Stephen 1986, Stephen 1987, Friedrich et al. 1988]. Obviously, the above desirable qualities and flexibilities make superplastic forming (SPF) with or without concurrent diffusion bonding (DB) a competitive industrial forming process compared with the other more conventional processes.

2. Basic Theory

2.1 Constitutive Law for Superplastic Deformation

The suggestion by Backofen, Turner and Avery[Padmanabhan et al. 1980] can be considered as the basis of superplastic flow. The important characteristic of the superplastic deformation, which applies to both 'structural' and 'environmental' superplasticities, is considerably associated with the dependence of the so-called flow stress σ on the deformation rate $\dot{\varepsilon}$, which resists the formation of localized necks during the course of the deformation process. Generally, the tensile test of a standard specimen is widely used for assessing the constitutive law of materials. In this test, the specimen is subjected to an axial (tensile) load and the elongation, generally, comprises three modes of deformations as follows [Padmanabhan et al. 1980]:

(a) An instantaneous elastic deformation that is recovered on the removal of loads,
(b) A time-dependent anelastic deformation that is also recoverable on the load removal,
(c) An irreversible plastic deformation that may contain both time-dependent and time-independent modes.

In the case of superplastic deformation, it can be argued that the elastic and anelastic modes are generally insignificant as far as superplastic elongations are concerned, which are typically between 200% and 1000%. Furthermore, the inducement of superplasticity at temperatures of approximately half of the melting point of the materials and at a rather slow deformation rate is unlikely to produce unwanted elastic effects such as spring-back effects. Several forms of the constitutive laws to evaluate the dependence of the flow stress on the strain rate for superplastic materials have been suggested in reference 1. A general constitutive law based on plastic deformation states that the flow stress (σ) is considered an instantaneous function of strain (ε), strain rate ($\dot{\varepsilon}$) and temperature (T) and reads as follows:

$$\sigma = f(\varepsilon, \dot{\varepsilon}, T) \tag{3}$$

where $\varepsilon = \int \dot{\varepsilon}\, dt$

For straining under isothermal conditions, which are typical for superplastic forming operations, equation (3) reduces to:

$$\sigma = f(\varepsilon, \dot{\varepsilon}) \tag{4}$$

Which in general form is often expressed in a power law type of equation, as follows:

$$\sigma - \sigma_y = K \varepsilon^n \dot{\varepsilon}^m \tag{5}$$

Where n is the strain hardening coefficient; m is the strain-rate sensitivity index; K is a material constant; and σ_y is a limit stress or 'threshold' stress that indicates the onset of flow. In the case of superplastic deformation, it is reported that strain hardening is usually negligible, and the 'threshold' stress, σ_y, is low and may be neglected due to experimental measurement uncertainties[1)]. Consequently, instead of equation (5), the simplified constitutive relation of the form:

$$\sigma = K\dot{\varepsilon}^m \tag{6}$$

is generally accepted for the description of superplastic flow that is in conformity with that suggested by Backqofen, Turner and Avery[Padmanabhan et al. 1980]. Furthermore, under multiaxial stress conditions, equation (6) may be considered as the relation between the von Mises equivalent stress σ and the equivalent strain rate $\dot{\varepsilon}$, and it reads as follows [Padmanabhan et al. 1980, Pearce 1987, Hamilton 1988]:

$$\overline{\sigma} = K\dot{\overline{\varepsilon}}^m \tag{7}$$

The important characteristics of superplastic materials are schematically depicted in Figure 4.

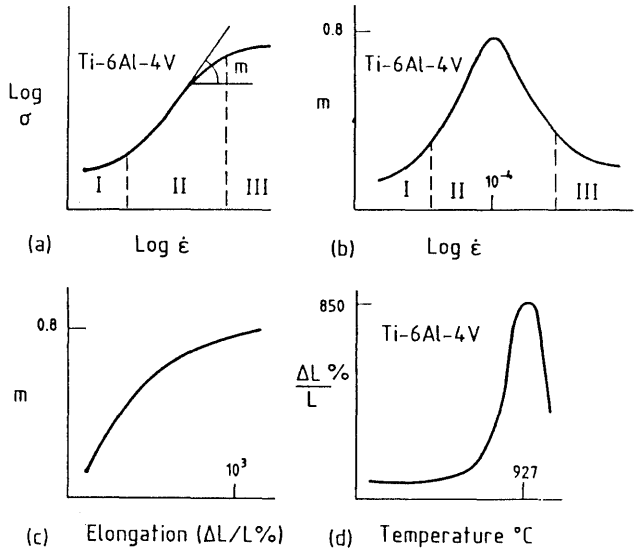

Figure 4. Typical Characteristics of Superplastic Materials

Region II in Figure 4, where the logarithmic relation of the constitutive law is almost linear, describes the strain-rate over which superplasticity occurs. This shows that superplastic materials are highly strain-rate sensitive and necessitate that the strain- rate be controlled during the deformation process so that a high strain-rate sensitivity index can be maintained to obtain high elongations. However, in Regions I and III, relatively small strain-rate sensitivity indexes are obtained. Since the elongation is also sensitive to temperature, as shown in Figure 4, it is necessary to control the temperature so that the deformation process takes place within a narrow temperature range. If the above process parameters are maintained during the deformation process, then, unlike conventional forms of ductile deformation, localized necking could be minimal.

3. Method and Materials

For SPF and SPF/DB to be successful, it is necessary to have a sound understanding of the process parameters involved, such as the problems of predicting the relationship between the forming pressure cycle and the final component configuration (including thickness distribution) and the effect of lubricant and bonding interactions. In addition, since every component is designed to satisfy certain structural and other environmental conditions, it may be necessary to device an initial distribution of sheet thickness to obtain the desired final thickness distribution. Additionally, in the case of superplastic forming/diffusion bonding (SPF/DB), the location of webs and web thickness information are necessary for designing structural components formed using this method. It is in this regard that the predictive capabilities of the finite element method can make a valuable contribution to the design of an SPF manufacturing process. Superplastic sheet forming is a process involving large deformation, large strain and, usually, deformation dependent boundary condition[19,20,27,28]. The deformation dependent boundary conditions originate from two sources, namely die-sheet and intersheet contact boundary conditions. Consequently, the numerical analysis of such a highly nonlinear transient process demands a formidable computational effort. Fortunately, the identification of the superplastic behaviour of metals as being characterized by the dependence of the flow stress upon the rate of strain (i.e., highly strain rate sensitive materials) has led to the recognition of similarities between this type of material response and that of a non-Newtonian viscous fluid[23]. This allows the possibility of developing a 'viscous flow' formulation to analyse superplastic forming processes, which overcomes many of the complexities associated with a large deformation solid mechanics-based approach [Zienkiewicz 1984, Jordaan et al. 2019].

3.1 Governing Equations and Optimized Rate of Deformation Control

In this paper, the sheet is modelled as a non-Newtonian viscous membrane for which the constitutive relation between the Von Mises equivalent stress σ and the equivalent strain rate $\dot{\varepsilon}$ is given in terms of viscosity μ as [Hamilton 1988, Askeland 1984, Ghosh et al. 1979, Kaibyshev et al. 2006, Jin 2019],

$$\overline{\sigma} = 3\mu\dot{\overline{\varepsilon}} \quad ; \quad \mu = \frac{K}{3}\dot{\overline{\varepsilon}}^{(m-1)} \tag{8}$$

where the constant K and the strain rate sensitivity index m. Incorporating plane stress and incompressibility assumptions enables the constitutive relations for membrane mechanics to be written as [Zienkiewicz 1984],

$$\sigma^{\alpha\beta}{}_m = 2\mu t\, C^{\alpha\beta\lambda\delta}\; D^m{}_{\lambda\delta} \qquad (9)$$

where in terms of convected coordinates ξ^α (α =1,2), $\sigma^{\alpha\beta}{}_m$ is the membrane stress resultant over thickness t, $D^m{}_{\lambda\delta}$ is the membrane rate of deformation and $C^{\alpha\beta\lambda\delta}$ is a function of the metric tensor. The governing equilibrium expression is the virtual velocity (rate of deformation) equation [Zienkiewicz 1984],

$$\int_A \sigma_m^{\alpha\beta}\,\delta D^m_{\alpha\beta}\,dA - \int_A p\,\delta v_3\,dA = 0 \qquad (10)$$

where A is the current sheet surface area, p is the pressure, and v_3 is the velocity normal to the sheet.

3.2 Optimized Rate of Deformation Control

To control the optimal rate of deformation within the superplastic material behavior, i.e., to introduce a pressure control schedule during superplastic forming, the equilibrium equation is augmented by an equation that constrains the maximum effective strain rate $\dot{\bar{\varepsilon}}_o$ as [Bonet et al. 1989],

$$L\,(\mathbf{D}(\mathbf{v})) = \dot{\bar{\varepsilon}}_o \qquad (11)$$

where L is a suitable function, weighting the strain rates **D**. Discretization of the virtual velocity equation, using 3-node constant stress triangular elements, yields a system of nonlinear differential equations in time as,

$$\mathbf{T}(\mathbf{x},\mathbf{v}) - \mathbf{F}(\mathbf{x},t) = 0 \qquad (12)$$

are solved using an implicit time stepping scheme, see Figure 5, which, on account of the geometric and material nonlinearity involved, requires the use of a Newton-Raphson iteration, summarized, in conjunction with Figure 5 for iteration k and time step (n+1) as

$$KT^k_{n+1}\Delta v^k_{n+1} = F(x^k_{n+1}, t_{n+1}) - T(x^k_{n+1}, t^k_{n+1}) \quad ; \quad v^{k+1}_{n+1} = v^k_{n+1} + \Delta v^k_{n+1} \qquad (13)$$

where the tangent stiffness matrix KT for iteration k and time step (n+1),

$$KT^k_{n+1} = \frac{\partial T}{\partial v^k_{n+1}} + \left[\frac{\partial T}{\partial x^k_{n+1}} - \frac{\partial F}{\partial x^k_{n+1}}\right]\frac{\partial x^k_{n+1}}{\partial v^k_{n+1}} \qquad (14)$$

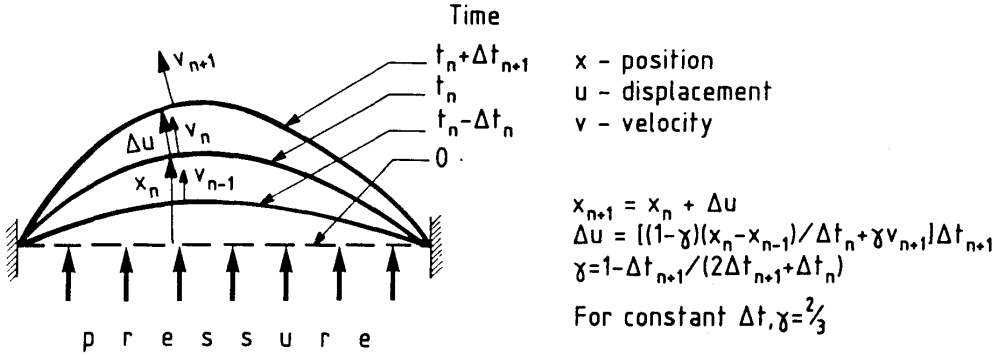

Figure 5. The Implicit Time Stepping Scheme

3.3 Contact mechanics with molds and contact between plate materials

The mechanics of the contact between the plate material and the mold (die-sheet contact) are completed using the penalty control method. Contact between plate material parts to model the influence of diffusion bonding is also resolved by the penalty control method, where the parts of the plate that contact each other are considered to have perfect sticking contact during the process. This condition is achieved by generating countercontact forces and minimizing penetration.

The surfaces of these interconnected parts of the plates (the neighboring parts) are called the 'master' face and the 'slave' face. The penetration vector **p** and the penetration velocity vector $\mathbf{v}_p$ are expressed as the relative position and relative deformation velocity of the 'slave' point that is outside the mold against the penetration point on the 'master' surface as follows (see Figure 6):

$$\mathbf{p} = \mathbf{x}_s - \mathbf{x}_p \quad (15)$$

$$\mathbf{v}_p = \mathbf{v}_s - \mathbf{v}_p \quad (16)$$

The contact force $\mathbf{B}_s$ acting at the 'slave' point s is expressed as a function of the penalty stiffness value k and the penalty viscosity c, while the contact force equal in magnitude but in the opposite direction to $\mathbf{B}_s$ acts on the 'master' element distributed as the forces at the point of the equivalent node $\mathbf{B}_m$. The kinematics of the contact forces on the 'master-slave' interface can be seen in Figure 6. The contact forces between plates $\mathbf{B}_s$ and $\mathbf{B}_m$ are as follows [Bonet et al. 1989, Zienkiewicz 1984, Wargadipura 1999]:

$$\mathbf{B}_s = -\left(k\,\mathbf{p} + c\,\mathbf{v}_p \right) \quad (11.a)$$

$$\mathbf{B}_s = \left(k\,\mathbf{p} + c\,\mathbf{v}_p \right)\mathbf{N}(\xi) \quad (11.b)$$

By incorporating the contact forces above (known as 'boundary' contact forces) in the equilibrium equation, the final form of the equilibrium equation that must be achieved is as follows[Bonet et al. 1989, Zienkiewicz 1984, Wargadipura 1999]

$$\mathbf{T}(\mathbf{x},\mathbf{v}) = p(t)\,\mathbf{F}(\mathbf{x},t) + \mathbf{B}(\mathbf{x},\mathbf{v}) \quad (12.a)$$

$$L(\mathbf{x},\mathbf{v}) = \mathrm{Max}\left(\dot{\bar{\varepsilon}}^{e} \right) = \dot{\bar{\varepsilon}}_o \quad (12.b)$$

in which $\mathbf{B}(\mathbf{x},\mathbf{v}) = \mathbf{B}_m + \mathbf{B}_s$ is the contact boundary force at the interface of the contacted plate material.

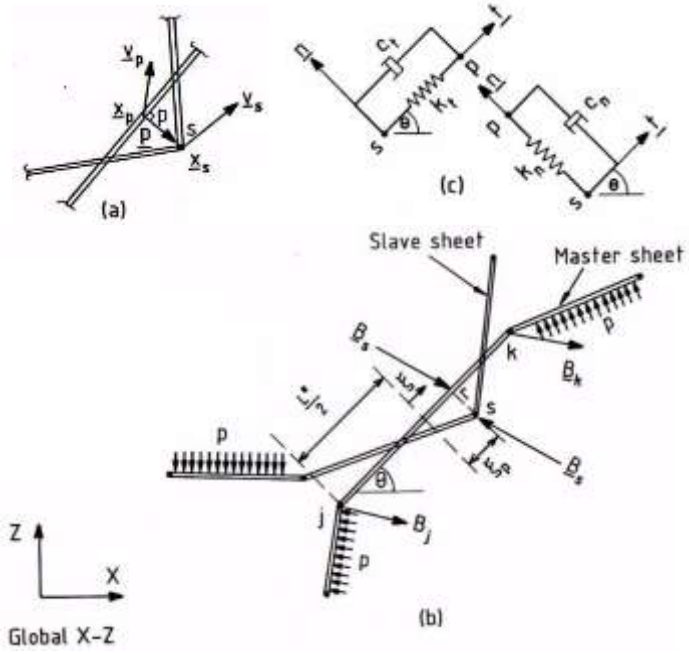

Figure 6. Intersheet material (interface master-slave) kinematics

3.4 Numerical Solution Technique and Procedure

Equation (12. a,b) is a set of differential equations in the time function and given the constitutive (material) equations used, as well as the SPF process itself. Then, the differential equation is a nonlinear function of position (geometry) **x**, deformation velocity **v** and forming pressure p. To follow changes in the shape of the plates during the superplastic deformation process, it is necessary that the geometric position **x** is connected with the deformation velocity **v** through the numerical integration of time (time stepping), which transforms the differential equations in the time function into a set of algebraic equations. Furthermore, these algebraic equations are solved in a time step series so that changes in the geometry of the plates can be followed. For this purpose, an implicit time integration technique, i.e., a predictor-corrector procedure, was developed, where the corrector stage is essentially a Newton-Rhapson nonlinear solution technique, as shown in Figure 7.

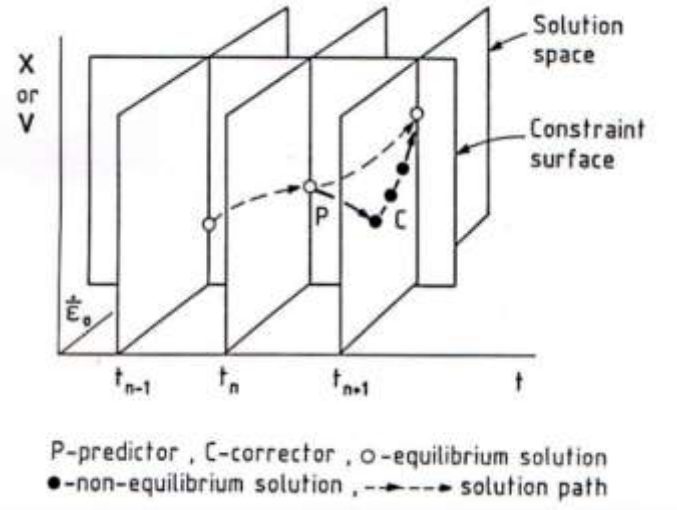

Figure 7. Predictor-Corrector Procedure

The numerical solution procedure of the governing equation for superplastic metal forming (SPF) processes, including diffusion bonding (DB) effects, is as follows:

Step I. Set Initial Conditions; $t_0 = 0, \rightarrow n = 0$, $\mathbf{v}_0 = 0$, $\mathbf{x}_0 = 0$, $p_0 = 0$

Step II. Time step Loop : $t_{n+1} = t_n + \Delta t$

Predictor: $\mathbf{v}^{\circ}_{n+1} = \mathbf{v}_n$; $\mathbf{x}^{\circ}_{n+1} = \mathbf{x}_n + \mathbf{v}_n.\Delta t$, $p^{o}_{n+1} = p_n$

For each material node and each 'slave' node, check the penetration through the die boundary and 'master' segment, respectively.

Step III. Nonlinear iteration loop: k = 0

Corrector:

1. Compute Residual Force: $\mathbf{R}^k = p^k_{n+1}\,\mathbf{F}(\mathbf{x}^k_{n+1},\mathbf{t}_{n+1}) + \mathbf{B}(\mathbf{x}^k_{n+1},\mathbf{v}^k_{n+1}) - \mathbf{T}(\mathbf{x}^k_{n+1},\mathbf{v}^k_{n+1})$
   (i.e., the boundary forces **B** are activated if contacts exist between the workpiece material and the die surface as well as interactions among the workpiece materials/ *interface master-slave*)
2. Compute strain rate error: $S^k = \dot{\bar{\varepsilon}}_o - e^{max}\left\{\frac{\dot{\bar{\varepsilon}}_e}{\dot{\bar{\varepsilon}}_k}\right\}$
3. Compute error norm: $E_1 = \| \mathbf{R}^k \| / \| p^k_{n+1}\,\mathbf{F}^k_{n+1} \|$ and
   $E_2 = \| S^k \| / \dot{\bar{\varepsilon}}_o$
4. Check convergence: If $E_1 \le \delta_1$ dan $E_2 \le \delta_2$ go to **Step IV**
5. Compute tanget matrix: $\mathbf{K}^k_t$
6. Compute constraint gradient vector $\mathbf{L}^k$
7. Compute $\boldsymbol{\psi}^k_1 = \left[\mathbf{K}^k_t\right]^{-1}\mathbf{R}^k$ and $\boldsymbol{\psi}^k_2 = \left[\mathbf{K}^k_t\right]^{-1}\mathbf{F}^k$
8. Solve for $\Delta p^k = \{ S^k - (\mathbf{L}^k)^T \boldsymbol{\psi}^k_1 \} / \{ \mathbf{L}^k \}^T \boldsymbol{\psi}^k_2$
9. Solve for $\Delta \mathbf{v}^k = \boldsymbol{\psi}^k_1 + \Delta p^k \boldsymbol{\psi}^k_2$
10. Update variabel: $\mathbf{v}^{k+1}_{n+1} = \mathbf{v}^k_{n+1} + \Delta \mathbf{v}^k$
    $\mathbf{x}^{k+1}_{n+1} = \mathbf{x}_n + \tfrac{1}{2}(\mathbf{v}_n + \mathbf{v}^{k+1}_{n+1}).\Delta t$
    $p^{k+1}_{n+1} = p^k_n + \Delta p^k$
11. Check for penetration of each work-piece material node through the die boundary and contact boundary at the interface master-slave of interacting work-piece materials.
12. Set $k \leftarrow (k+1)$ dan return to 1.

Step IV. Output variables: t_{n+1}, $\mathbf{v}_{n+1}$, $\mathbf{x}_{n+1}$, p_{n+1}

Step V. Set n ← (n+1) and return to **Step II** or stop the process if the full contact condition or the maximum number of time steps are reached.

3.5 Material

An experiment of superplastic forming of hydraulic bulging of the 7475 aluminum sheet alloy was attempted using the superplastic forming pressing machine to test the finite element viscous flow formulation developed herein to predict the behavior of the 7475 aluminum thin sheet during superplastic deformation processes. In this case, the chemical element mapping and composition were carried out using an X-ray fluorescence (XRF) metal analyser, and the resulting XRF chemical element mapping and composition may be seen in Figure 8 and Table 2, respectively.

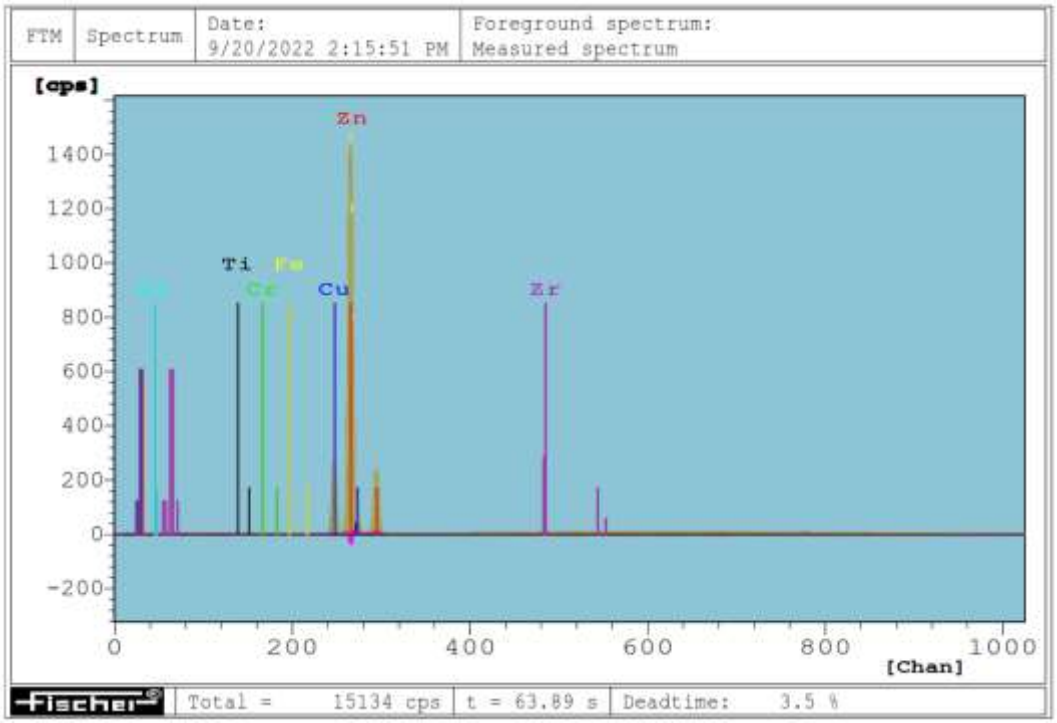

Figure 8. Chemical Element Mapping of the 7475 Aluminum Alloy using XRF

The chemical element composition of the 7475 aluminum alloy used herein measured by the XRF metal analyser may be seen in Table 2.

Table 2. Chemical Composition of the 7475 Aluminum Alloy

	Foreground: Measured spectrum
	Scattering spectrum
	Sum of spectra
	Residual
Meas. para. (foreground spectrum):	
High voltage = 50 kV (875)	Prim. Filter = Al1000
Collimator 1 = 1.00 Dm.	Anode current 1000 uA
Meas. distance = 3.73 mm	
FastC = 15177.49, SlowC = 14645.29	
Results of analysis: (%)	
30 Zn	= 9.22
29 Cu	= 2.19
24 Cr	= 0.28
26 Fe	= 0.14
22 Ti	= 0.31
40 Zr	= 0.04
13 Al	= 87.82

4. Results and Discussion

4.1 Validation of Finite Element Formulation and Rate of Deformation Control Algorithm

The validation of the finite element formulation employing viscous flow mechanics together with the rate of superplastic deformation control algorithm is attemped by the free forming of a plane-strain thin-sheet of a typical superplastic material with constant values of m=0,64 and K=1200 MPa.Sec.^{m}. The problem definition is given in Figure 9, and the convergence tolerance either for the residual force or the strain rate error/pressure is set at 0.1%. Assuming a circular bulge profile enables the pressure required to maintain the imposed equivalent strain rate to be approximated as follows.

Assuming a circular bulge profile with the sheet thickness hand radius R in which membrane behaviour prevails enables the stress equilibrium (see Figure 9) to be written as,

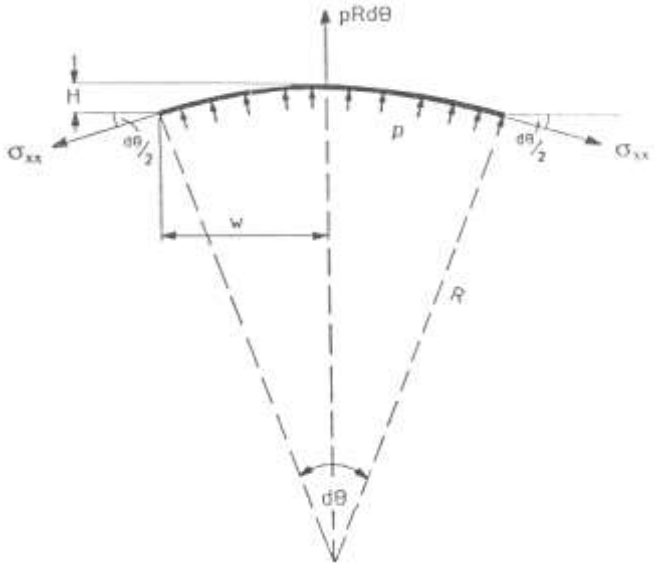

Figure 9. Geometry of Deformation

$2\times\sigma_{xx} h\frac{d\theta}{2} = pRd\theta$, giving the pressure $p = \frac{\sigma_{xx} H}{R}$ (13)

Using the constitutive equations under the plane strain condition of $\sigma_{xx} = 4\mu\dot{\varepsilon}_{xx}$ dimana $\mu = \frac{K}{3}\dot{\bar{\varepsilon}}^{(m-1)}$ enables the stress in the width direction σ_{xx} to be evaluated as follows:

$\sigma_{xx} = 4\mu\dot{\varepsilon}_{xx}$ and substituting the value of $\mu = \frac{K}{3}\dot{\bar{\varepsilon}}^{(m-1)}$ results in $\sigma = \frac{2}{3}\sqrt{3}K\dot{\bar{\varepsilon}}^m$, where $\dot{\varepsilon}_{xx}$ and $\dot{\bar{\varepsilon}}$ are strain-rate in the width direction and the equivalent strain rate, respectively. Substituting the equation of $\sigma = \frac{2}{3}\sqrt{3}K\dot{\bar{\varepsilon}}^m$ into the equation of $p = \frac{\sigma_{xx} H}{R}$ and imposing the rate of deformation control in terms of the equivalent strain rate control $\dot{\bar{\varepsilon}} = \dot{\bar{\varepsilon}}_o$ enables the forming pressure to be evaluated as,

$$p = \frac{2}{3}\sqrt{3}\frac{H}{R}K\dot{\bar{\varepsilon}}_o^{\ m} \quad (14)$$

where $\dot{\bar{\varepsilon}}_o$ is the imposed equivalent strain rate, h is the thickness of the plate, H is the bulge height, W is the semiwidth of the sheet, and R is the bulge radius. the radius R may be approximated (see Figure 9) as follows.

$R^2 = W^2 + (R-H)^2$, results in $R = \frac{W^2 + H^2}{2H}$ (15)

where W and H are the semiwidth and bulge height of the sheet, respectively.

4.1.1 Hydraulic Free Bulging of Thin Strip Plate

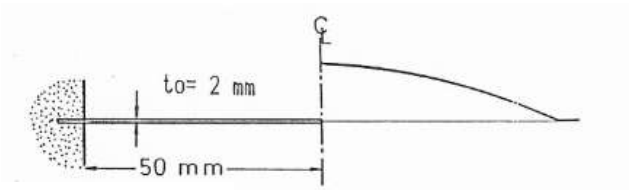

Material Properties: K=1200 MPa.Sec^m.

M=0.64

Initial Pressure: p_o=0.030 MPa.

Maximum Strain Rate: $\dot{\bar{\varepsilon}}$ =0.00030 sec^{-1}

Figure 10. Problem Definition of Hydraulic Bulging of Sheet Plate

The deformed shape of the sheet at various times, the profile of the pressure cycle computed using the finite element formulation developed and the computed maximum equivalent strain-rate are depicted in Figure 11.

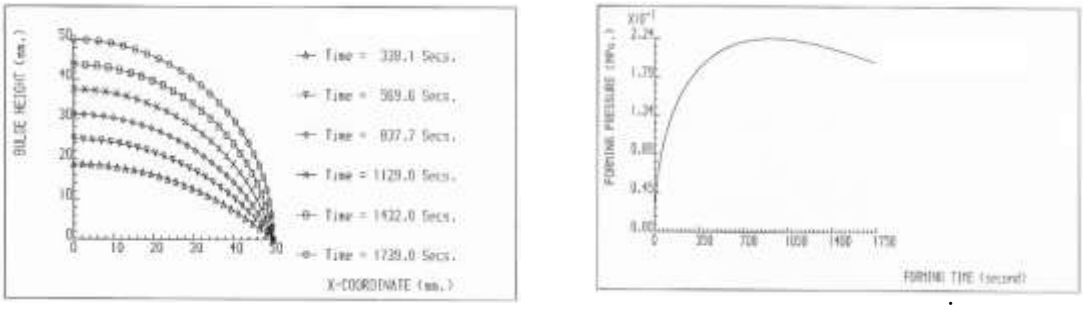

(a) Deformed Shape at Various Time **(b) Pressure Cycle Profile for Max $\dot{\bar{\varepsilon}}_o$=3 x 10^{-4}sec^{-1}**

Figure 11. Deformed Shapes and Pressure Cycle for Maximum Equivalent Strain Rates

The numerical comparisons for the pressure between the approximate analytical solution calculated using equation (14) and the finite element solution employing the implicit time integration scheme are given in Table 3, as follows.

Table 3. Comparison between Approximate Analytical Solution and F.E. Solution

No.	Sheet Geometry		Approximate Analytical Solution	Finite Element (FE) Solution	Error (%)
	Bulge Height (mm)	Thickness (mm)	Pressure (MPa.)	Pressure (MPa.)	
1	6.3997	1.9787	0.0768	0.0777	1.17
2	12.5752	1.9202	0.1400	0.1404	0.28
3	18.7821	1.8324	0.1860	0.1862	0.11
4	25.0085	1.7254	0.2129	0.2129	0.00
5	31.2449	1.6094	0.2230	0.2231	0.04
6	37.4877	1.4922	0.2209	0.2209	0.00
7	43.7347	1.3792	0.2108	0.2108	0.00
8	49.9846	l.2735	0.1964	0.1964	0.00

As can be seen from Table 3, the computed pressure to maintain the imposed equivalent strain-rate $\dot{\bar{\varepsilon}}_o$=3,0 x 10^{-4} sec^{-1} compares very well with the approximate solution based on thin-sheet membrane theory, and it gives the computed maximum equivalent strain-rate, which confirms that the strain-rate constraint of $\dot{\bar{\varepsilon}}_o$=3,0 x 10^{-4} sec^{-1} is working correctly, as shown in Figure 11.

4.2 The Superplastically Formed Aluminum 7475 Hemispherical Dome.

The experimental work was carried out using a superplastic forming/diffusion bonding (SPF/DB) pressing machine, as depicted in Figure 12. It is shown that a true hemispherical dome geometry made of the 7475 aluminium sheet alloy could be formed out of the flat sheet. Four configurations of the hemispherical dome were obtained in the experiment. In this paper, the result obtained for the forming period of 9.0 minutes is investigated and compared with the finite element simulation using the 'viscous flow' formulation discussed earlier. In this case, the dome configuration with the ratio of bulge height (H) to die-entry diameter (D), i.e., H/D ratio of 42.13%, is obtained and shown in Figure 13.

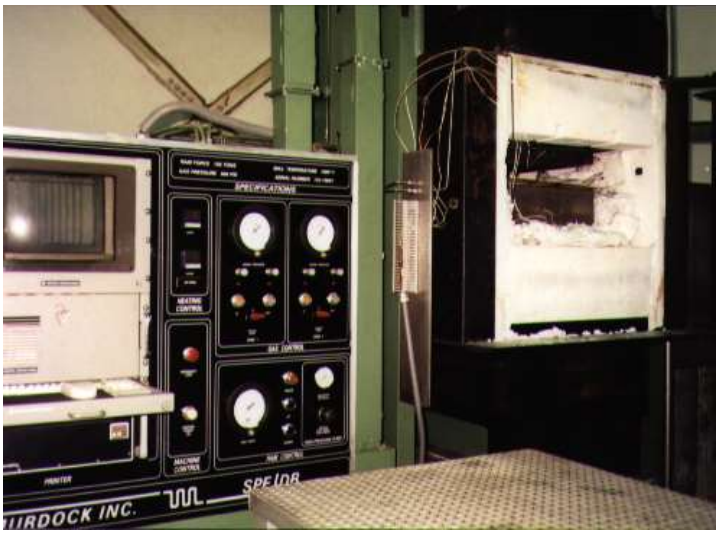

Figure 12. The SPF/DB Pressing Machine used

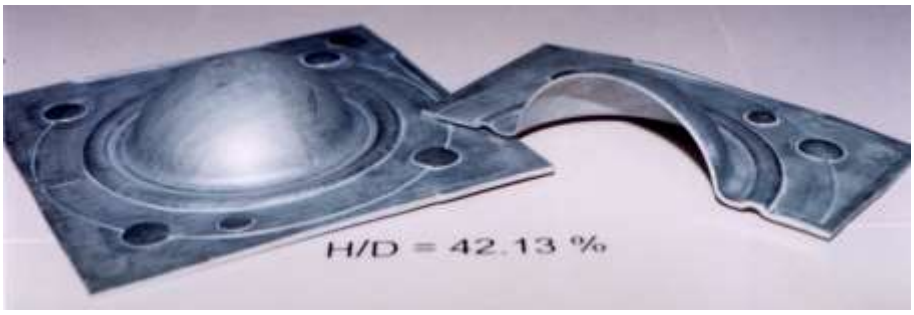

Figure 13. Superplastically Formed Hemispherical Dome Components Al-7475

The thickness and bulge height of the formed hemispherical components were measured along the diametric arch on the bulge profile by sectioning the hemispherical dome. The results of the thickness and bulge height measurements of the formed hemispherical dome component are given in Table 4.

Table 4. Thickness and Bulge Height Measurement for H/D = 42,13%

Dome Geometry Configuration	**Sheet Thickness (mm.)**					**Bulge Height (mm.)**				
	T_1	T_2	T_3	T_4	T_5	T_1	T_2	T_3	T_4	T_5
H/D= 42,13 %	1,375	1,409	1,452	1,497	1,660	31,60	30,35	26,0	22,50	14,60

Note that T_1, T_2, T_3, T_4 and T_5 are the locations in a flat blank sheet measured beginning from the center of the circle outwards in a radial direction with 7.50 mm spacing. It should also be noted here that some slippage of the sheet material held between the upper and lower dies could also take place during the entire forming period. To study the deformation process during the forming period, a finite element model using the viscous shell formulation described earlier is developed. The pressurization schedule is taken to be the same as that used in the experimental investigation. The superplastic material parameter, K and strain rate sensitivity index, m, of the 7475 aluminum sheet alloy are determined herein based on the uniaxial tensile test of 7475 aluminum at the superplastic temperature of 515–525^{o}C using a high temperature furnace [Wargadipura 1999]. In this case, the material parameter K = 2.0 MPa. Sec^{m} and the strain rate sensitivity index m = 0.304. The graphical plots of the comparison between the

experimental and computed results, in terms of the bulge profiles and the thickness distributions, are depicted in Figure 14(a) and Figure 14(b), respectively.

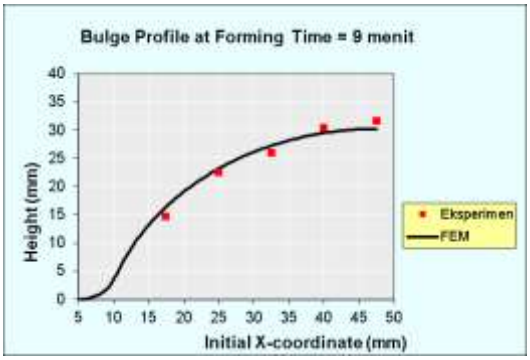

(a) Bulge Height Profile

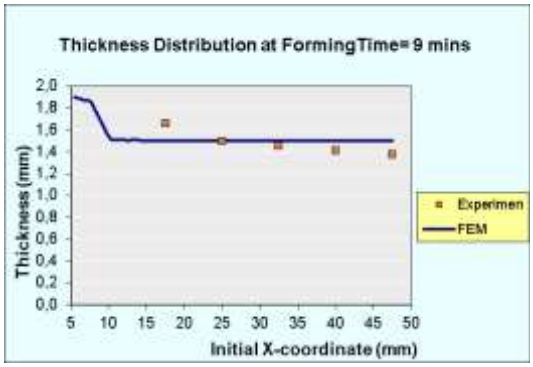

(b) Thickness Distribution

Figure 14. Experimental and Finite Element Results (H/D= 42.13%)

As seen from Figure 14(a), the finite element computed bulge height, in general, compares very well with the bulge height obtained from the experimental result for 9.0 minutes of forming time. The thickness distribution along the diametric arch on the bulge profile for different forming times obtained from the experimental and finite element results is shown in Figure 14(b). In this case, the thickness distribution is plotted against the initial diametric flat position. As seen in Figure 14(b), the thinning process of the sheet material obtained from the experimental result increased from the edge to the pole, where the strain reached its maximum value as the forming time progressed. This thinning characteristic also applies to the computed thickness distribution, as shown in Figure 14(b). However, since sticking contact is used in the finite element model, the computed thinning of the sheet material is immediately frozen at the point of contact, and as the forming time progresses, thinning continues only in the uncontacted (free) region. Therefore, the minimum computed thickness occurs in the pole region of the hemispherical dome, while in the edge (clamped) region where the sheet material subsequently contacted the die surface, the edge thickness of the sheet has a higher value and is not uniformly distributed. In addition, some material slippages can also take place in the edge (clamped) region of the sheet diaphragm. This situation also contributes to the differences between the experimental and finite element results. However, in general, the finite element model could significantly follow the thinning behaviour of the sheet material.

4.3 Simulation of SPF/DB of a Multicell NACA 0012 Aerofoil Section

This application concerns the core sheet forming of the four-sheet SPF/DB process as described previously. Herein, a four-cell NACA 0012 aerofoil section [I-Chung et al. 1995, Ira et al. 1959] is formed, allowing diffusion bonding between neighboring sheet materials to take place during forming. The equal cell pressure is constrained so that the maximum equivalent strain-rate is maintained at $\dot{\bar{\varepsilon}}_o = 0.00030$ sec^{-1}. Due to the symmetry of the problem, only half of the aerofoil section is considered, and all contact conditions are sticking contacts. The problem definition is given in Figure 14, and the convergence tolerance either for the residual force or the strain rate error/pressure is set at 0.1%.

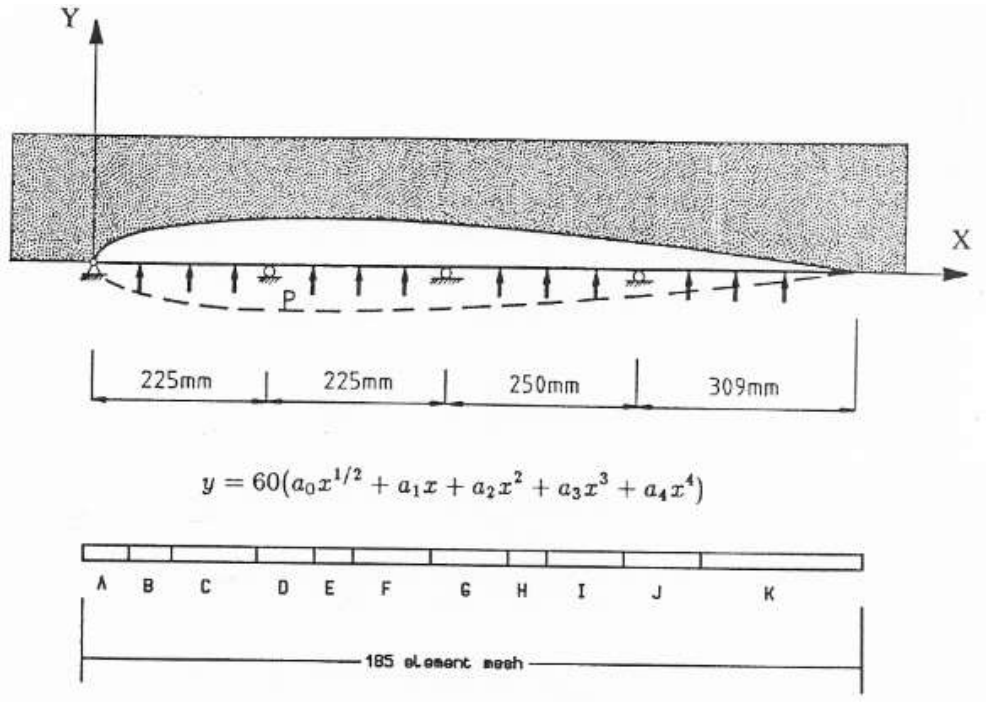

F.E. Mesh Division

A = 10 elements – 60.0 mm
B = 4 elements – 55.0 mm
C = 22 elements – 110.0 mm
D = 17 elements – 75.0 mm
E = 5 elements – 50.0 mm
F = 17 elements – 100.0 mm
G = 23 elements – 100.0 mm
H = 5 elements – 50.0 mm
I = 22 elements – 100.0 mm
J = 25 elements – 100.0 mm
K = 35 elements – 209.0 mm

Figure 15. Problem Definition of SPF/DB of the four-cell NACA 0012 aerofoil section

The computed pressure cycle for the controlled strain rates $\dot{\bar{\varepsilon}}_o$ = 3,0 x 10^{-4}sec^{-1} and the final thickness distribution are depicted in Figure 16(a) and Figure 16(b), respectively.

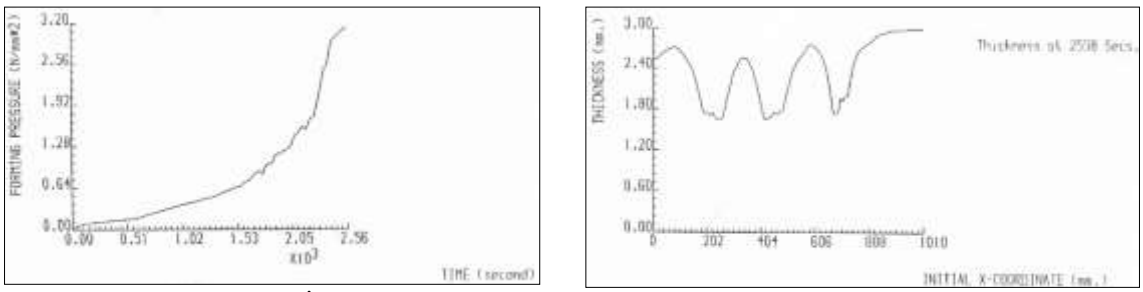

(a) Pressure Cycle for $\dot{\bar{\varepsilon}}_o$ = 3 x 10^{-4}sec^{-1} (b) Final thickness distribution

Figure 16. Pressure Cycle and Final Thickness Distribution

As shown in Figure 16(a), a slight drop in the pressurization during forming is observed. As observed before and checked in this application, the maximum equivalent strain-rate moved from one cell to another, causing the temporary drops in forming pressure to maintain $\dot{\bar{\varepsilon}}_o$ = 3,0 x 10^{-4}sec^{-1}.

The formed shapes at various forming times are presented in Figure 17. The simulation took 239 steps, with the forming time being completed in 42 minutes 38 seconds.

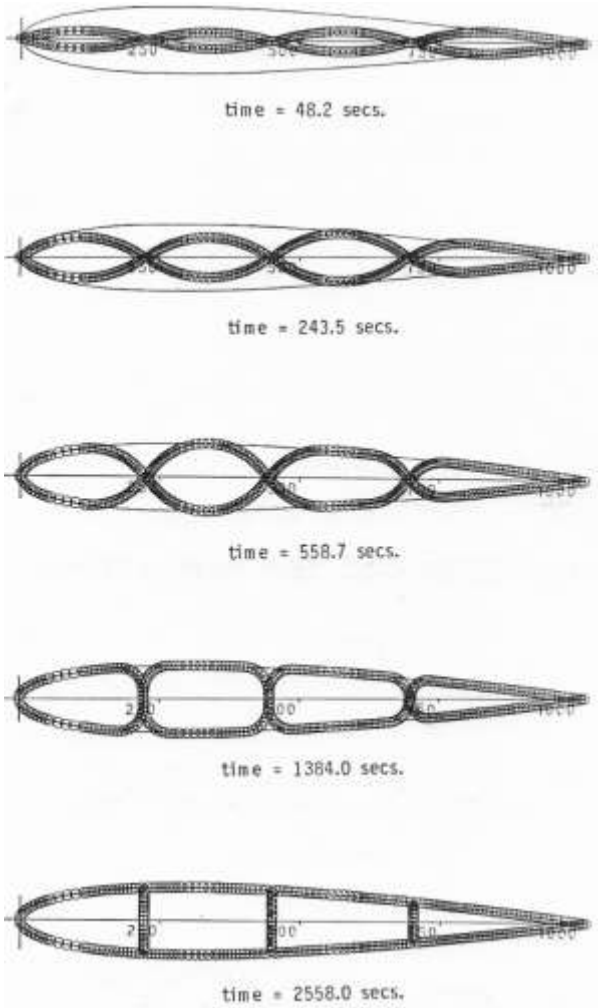

Figure 17. SPF/DB of a Multicell NACA 0012 Aerofoil Section – Formed Shapes

5. Conclusions

The characteristics of superplastic behaviour are such that the material can be represented as a non-Newtonian viscous fluid in which elastic effects are ignored. Such an approach results in the so-called 'viscous flow' formulation. Equilibrium equations were established using a rate form of the principle of virtual work, which, upon discretization, yields a set of differential equations in time. These equations, if desired, can be augmented by a scalar strain-rate constraint equation that constrains the rate of deformation so that the material maintains an optimum superplastic response. Based on this principle, a finite element 'viscous flow' formulation has been developed and applied to numerically simulate superplastic forming processes, including the diffusion bonding effect. The implementation of the 'viscous flow' formulation into a computer program has provided an analytical design tool capable of predicting the relationship between forming pressure and product shape, including thickness distributions and the effect of diffusion bonding. Using this methodology, it is possible to gain an in-depth understanding of the SPF and SPF/DB flexibilities and limitations that are required by the forming engineers if the maximum benefits of the SPF and SPF/DB are to be realized. The validation of the finite element viscous flow formulation was successfully carried out. The finite element calculations were checked against analytical solutions for free bulging of a strip. The results of finite element computation compare very well with the approximate solution of the bulging of a strip and the computed maximum equivalent strain-rate, which confirms that the strain-rate constraint of ε_o = 3,0 x 10^{-4} sec^- is working correctly. The experiment of superplastic forming of thin-sheet 7475 aluminum alloys into hemispherical dome shape has been successfully accomplished at a temperature of 515° C. Using the sheet thermoforming process at the appropriate temperature and forming pressure; true hemispheres could be formed out of the 7475 aluminum flat sheet. It is observed from the formed hemispherical dome of the 7475 aluminum that the thickness variation of the component increases with increasing bulge height of the dome, i.e., the thinning process increases from the edge to the pole where the strain reaches its maximum value. In other words, the thickness strain at a certain location along the bulge profile increases as the bulge height to the die-base diameter (H/D) ratio increases. The comparison between the results obtained from the superplastic forming experiment and the result obtained from the finite element simulation shows that the bulge profile obtained compares well, while the differences in the thickness distributions are due to the sticking boundary used in the finite

element model. However, in general, the viscous shell formulation implemented in the computer program could significantly follow the geometry changes, including thickness distributions during the superplastic forming of the 7475 aluminium hemispherical dome. Superplastic forming of thin sheet components is an attractive manufacturing process for which the predictive capabilities of the finite element method can make a valuable contribution. The application examples presented in this paper show that a membrane element formulation can be developed to model SPF in order to provide the forming engineer with data on the forming history of the shape and thickness distribution. Although not shown, the program can also yield the equivalent strain, strain rate and flow stress history together with the evolution of the distribution of the grain size. In addition, the strain rate control algorithm enables pressure cycles to be found that optimize the superplasticity behavior of the material. Finally, it has been demonstrated that the SPF of multicell diffusion bonded aerofoil section components can, under the flow stress of plane strain conditions, be numerically modelled. Clearly, the correlation between the finite element and experimental results needs to be improved, but even in its present state, the computer simulation provides important quantitative information.

Acknowledgements: The first author gratefully acknowledges the support provided by the Riset Unggulan Terpadu V Programme, administered by the Ministry for Research and Technology, Republic of Indonesia.
Funding: This research received no external funding.
Conflicts of Interest: The authors declare no conflict of interest.

References

[1] Al-Naib T.Y.M. and Duncan J.L. (1970). *Superplastic Metal Forming*, *Journal of Mechanical Sciences,* 12, 1970, 463-477.
[2] Askeland D.R. (1984). *The Science and Engineering of Materials*, Brooks/Cole Engineering Division Publisher, Monterey, California, 1984, 111 and 231-232.
[3] Bonet, J. Wargadipura A.H.S, and Wood R.D. (1989). *A pressure cycle control algorithm for superplastic forming*', communications in Applied Numerical Methods, 5(2), 1989, 121-128.
[4] British Aerospace, (1992). *Manufacturing Resources*, British Aerospace PLC, Warton Unit, Warton Aerodrome, Preston, Lancashire, the United Kingdom.
[5] Friedrich H.E., Furlan R, Kullick, M (1988). *SPF/DB on the Way to the Production Stage for Ti and Al Applications within Military and Civil Projects*, in Superplasticity and Superplastic Forming, Proc. of Int. Conf. on Superplasticity and Superplastic Forming, Blaine, Washington, USA, eds. C.H. Hamilton and N.E. Paton, a Publication of TMS, 1988, pp. 649-664.
[6] Ghosh A.K. and Hamilton C.H. (1979). *Mechanical behaviour and hardening characteristics of a superplastic Ti-6A9 alloy*, Metallurgical Transaction A, 10A, 699-706.
[7] Ghosh A.K. and Hamilton C.H. (1982) *Influence of material parameters and microstructure on superplastic forming*, The Metallurgical Transaction A, 13A, 1982, pp. 733-743.
[8] Hamilton C.H. (1977). *Forming of Superplastic Metals*, Proc. of a Symposium of Formability, Analysis, Modelling and Experimentation, eds. S.S. Hecker et al., The Metallurgical Society of AIME Shaping and Forming Committee, Chicago, USA, October 1977. pp. 232-258
[9] Hamilton C.H. (1988). *Superplasticity and Superplastic Forming*, Proc. of Int. Conf., editors C.H. Hamilton and N.E. Paton, Semiah-moo, Blaine, Washington State, A Publication of TMS, August 1988.
[10] Hamilton, H (1987). *Superplastic sheet forming*, in NATO/Advisory Group for Aerospace Research and Development, Lecture Series No. 154, London, U.K., September 1987.
[11] I-Chung C, Francisco J. T, and Chee T (1995). *Geometric Analysis of Wing Sections*, NASA Technical Memorandum 110346, Ames Research Center Moffett Field, California, 1995.
[12] Ira H. A and Albert E. V D (1959). *Theory of Wing Section*, Directorate of Aeronautical dan Space Research, NASA, Dover Publications, Inc., New York, 1929.
[13] Jin H (2019). *Optimization of Aluminum Alloy AA5083 for Superplastic and Quick Plastic Forming*, Metallurgical and Materials Transaction A, 50A, August 2019
[14] Jordaan M. S. and Kok S. (2019). *Material model calibration for superplastic forming*, Inverse Problems in Science and Engineering, 27, 5, 589 – 607.
[15] Kyung J M and Ho-Sung L (2015). *Integrated Manufacturing of Aerospace Components by Superplastic Forming Technology*, Matec Web of Conference 30, EDP Sciences, 2015.
[16] Kawasakia M and Langdon T.G. (2015). *Developing Superplasticity in Ultrafine-Grained Metals*, Acta Physica Polonica A, 128,4
[17] Kaibyshev O. A. (2006). *Advanced superplastic forming and diffusion bonding of titanium alloy* Materials Science and Technology, 22 3.
[18] Leodolter, W (1986). *Production Implementation of Titanium Superplastically Formed/Diffusion Bonded Structure*, Proc. of the Int. Conference on Titanium Products and Applications, Titanium Development Association, 1986, 1107-1112.
[19] Li Z, Zhao B and Chen W, (2015). *Superplastic forming and diffusion bonding: Progress and trends*, Matec Web of Conference 21, EDP Sciences, 2015.
[20] Maehara Y, Komizo Y. and Landon T.G. (1988). *Principle of superplastic diffusion bonding: an overview*, Materials Science and Technology, 4 - 8, August 1988, 669-674.
[21] Pearce R (1986). *Developments in Sheet Metal*, in Sheet Metal Industries, April 1986, 188-192.
[22] Pearce, R. (1987). *Superplasticity - an overview*, in NATO/Advisory Group for Aerospace Research and Development, Lecture Series No. 154, London, U.K., September 1987.

[23] Partridge P.G. and Ward-Close C.M. (1989). *Diffusion Bonding of Advanced Materials*, Metals and Materials 5, 6, June 1989, 334-339.
[24] Padmanabhan, K.A. and Davies, G.J (1980). *Superplasticity*, Material Research and Engineering 2, Springer-Verlag, Berlin, 1980.
[25] Stephen, D. (1986). *Titanium Diffusion Bonding in the Manufacture of Aircraft Structure*, Proc. of the Int. Conf. on Titanium Products and Applications, Titanium Development Association, 1986, pp. 603-630.
[26] Stephen, D. (1987). *Designing for Superplastic Alloys*, in NATO/Advisory Group for Aerospace Research and Development, Lecture Series No. 154, London, U.K., September 1987.
[27] Valiev R. Z., Murashkin M.Y. and Semenova I.P. (2010). *Grain Boundaries and Mechanical Properties of Ultrafine-Grained Metals*, Metallurgical and Materials Transaction A, Volume 41A, April 2010.
[28] Wargadipura A.H.S (1999). *Laporan Riset Unggulan Terpadu V: Karakterisasi Superplastis Material Aluminium 7475*, Kelompok Rancang Bangun, Program Riset Unggulan Terpadu, Kementrian Negara Riset dan Teknologi.
[29] Williamson J.R. (1986). *Superplastic Forming/Diffusion Bonding of Titanium - an Air Force Overview*, Proc. of the Int. Conf. on Titanium Products and Applications, Titanium Development Association, 1986, pp. 1087-1106.
[30] Zienkiewicz O.C. (1984). *Flow formulation for numerical solution of forming processes*, in Numerical Analysis of Forming Processes, eds. Pittman et al., John Wiley & Sons, 1984, 1-44